Optimization of Draw-In for an Automotive Sheet Metal Part An evaluation using surrogate models and response surfaces

Jansson, T.; Andersson, Alf; Nilsson, L.

Published in:
Journal of Materials Processing Technology

DOI:
10.1016/j.jmatprotec.2004.06.011

2005

PAPER E

Optimization of draw-in for an automotive sheet metal part
- An evaluation using surrogate models and response surfaces

Optimization of draw-in for an automotive sheet metal part
– An evaluation using surrogate models and response surfaces

T. Jansson[a,*], A. Andersson[b,c], L. Nilsson[a]

[a]*Division of Solid Mechanics, Linköping University, Sweden*
[b]*Volvo Cars Body Components, Olofström, Sweden*
[c]*Division of Production and Materials Engineering, Lund University, Lund, Sweden*

Abstract

In the present paper, an optimization of the draw-in of an automotive sheet metal part has been carried out using Response Surface Methodology (RSM) and Space Mapping technique. The optimization adjusts the drawbead restraining force in the model such that the draw-in in the FE model corresponds to the draw-in in the physical process. The conclusion of this study is that Space Mapping is a very effective and accurate method to use when calibrating the draw-in of a sheet metal process. In order to establish drawbead geometry from the drawbead restraining force a 2D-model was utilized. The drawbead geometry found showed good agreement with the physical drawbead geometry.

Key words: Response Surfaces, Space Mapping, Sheet Metal Forming, Optimization, Simulation, Draw-in, Drawbead

1 Introduction

Finite Element (FE) simulations have become an efficient tool during the last decade for developing sheet metal forming processes. The most significant advantage compared to try-out methods are the time and cost reductions but also the deeper understanding of the mechanics involved. The utilization of sheet metal forming simulations in the automotive industry has been described by [1]-[3].

Today, forming simulations are mainly used with manual iterations to develop a process giving acceptable parts. Since the forming operation is complex, it must

* Corresponding author.
Email addresses: tomja@ikp.liu.se (T. Jansson), aander58@volvocars.com (A.Andersson) larni@ikp.liu.se (L. Nilsson).

be the object to eventually develop an efficient automated optimization of the forming process. One step to increase the use of mathematical optimization is to optimize process objectives by using the drawbead geometry as design parameters. Evaluations of the effect of drawbeads have been carried out by many authors [4]-[6]. Most Finite Element codes use an equivalent drawbead, which consists of a restraining force applied to the blank at the location of the drawbead. In this paper, the drawbead geometry is optimized such that the part fit a certain draw-in achieved in a try-out tool. Thereafter the equivalent drawbead force is transferred into a 2D-geometry for the evaluation of the physical shape of the drawbead. Today, this procedure is done manually, however a mathematical optimization algorithm would be more efficient and helpful.

The use of structural optimization has increased rapidly during recent years, mainly due to faster computers, better algorithms and more frequent use of FE simulations. Optimization is a useful tool to improve the design in a well structured manner. Structural optimization often uses gradients of the objective and constraints to find a search direction of the optimal solution. Nanceur et al. [7] used a one-step inverse code to optimize the restraining forces of the equivalent drawbeads with a gradient based optimization method. However, for nonlinear problems like sheet metal forming problems, the solution functions are often noisy and it is hard to find these gradients.

In the Response Surface Methodology (RSM) polynomial surfaces are fit to objective and constraint values in the design space. Due to the construction of these surfaces, noisy or unphysical components of the response will be smoothened out. The optimal solution is then searched on the smoothed surfaces, rather than on the real response surfaces. For further reading about RSM, see [8]-[10]. Kok and Stander [11] used RSM to optimize the thickness distribution in a formed part using the FE code LS-DYNA. Other examples of optimization in sheet metal forming can be found in [12]-[27].

Even if the number of evaluations is low, the computing time to evaluate each design can be distressingly long. There is a need for methods where simplified models can be used for most evaluations, such that the number of full model evaluations is minimized. The simplified models can be constructed using a coarse mesh, simplified numerical models, approximative analytic solutions etc.

One method, which makes this possible, is called Space Mapping (SM), where a surrogate model complements the full model. The surrogate model (coarse model) determines the search direction and the full model (fine model) will determine the design point for the next iteration. The use of the coarse model makes it possible to reduce the total computing time and the fine model assures an accurate solution.

Space Mapping and surrogate models have until recently been utilized in electromagnetic and circuit optimization, see e.g. [28]. Leary et al. [29] used Space Mapping in structural optimization of a simple cantilever beam. Redhe and Nilsson [30] used Space Mapping in structural optimization in crashworthiness design. A mathematical viewpoint of space mapping can be found in [31].

The algorithm used in this paper is a combination of RSM and SM. Initially one iteration with RSM is performed resulting in response surfaces of the objective and constraints. These response surfaces are then used as a coarse model in the subsequent SM iterations. The algorithm used is presented in Jansson et al. [32].

When the process produces a part with satisfactory properties the final parameter set-up must be transformed to a physical tool, e.g. each of the desired drawbead restraining forces must be transformed to a drawbead geometry. This is commonly done by comparing the draw-in in the simulation with the draw-in in the physical tool. The geometry of the drawbeads are adjusted until the draw-in from the simulation matches the physical draw-in.

The aim of this paper is to show that mathematical optimization using RSM and Space Mapping is an effective tool to use when the draw-in in a FE model is calibrated with the draw-in from a physical test and to evaluate the drawbead geometry based on the results.

2 Methodology

The experimental test to be analyzed is set up in order to determine the drawbead restraining forces with the aim of better understanding the drawbead mechanics in prediction of future forming processes. The methodology used for the experimental tests, forming simulation and for the optimization techniques are described below.

2.1 Methodology for the experimental tests

The chosen geometry is a well defined try-out tool, were CAD-data corresponds to the physical tool. No changes were made except for adjustments of hard points in the binder. Furthermore the drawbeads are designed in rather straight sections. This will decrease the difficulties with complicated restraining forces in a curved drawbead geometry due to in-plane compression/stretching of the material. The experimental test was performed in a hydraulic double action press, which gave opportunities to perform a well-controlled process.

In order to have a well-defined process to simulate, a blank holding gap of 0.1 mm was used during the forming process. Hence, the drawbeads will apply the restraining forces and the binder will apply a uniform pressure over the blank.

In order to calibrate the draw-in in the simulation one part was taken after the binder wrap. This part was used as a reference when the draw-in was measured after the final drawing. The draw-in was then measured as the change in flange length between binder wrap and final shape on several positions. In order to have the correct position after binder wrap also the flange length after binder wrap was measured and compared to the simulation results. Furthermore the punch force was registered in order to compare with simulation results.

Three parts were evaluated in order to have knowledge of the scatter in the experimental results.

The methodology is described in Figure 1 together with the methodology for the forming simulation.

2.2 Forming simulation methodology

The methodology for the forming simulation is described in Figure 1. First the mechanical properties of the material were obtained from a tensile test.

Based on the CAD geometry an FE model was created. The simulation was divided into three steps:

1. Gravity loading
2. Binder wrap
3. Forming, excluding unloading

In step 1 and 2 a coarse mesh was used in order to save computing time. The only parameter which was changed during the first two steps was the initial blank positioning. The two first steps were looped manually until convergence with experimental results was achieved. After convergence the sheet metal forming process was simulated with a refined model from step 2 and the results were compared with the results achieved from the experiments. In step 3 the drawbead restraining force was optimized. If the results differed, a new set of drawbead restraining forces was applied and step 3 was looped until convergence was found. This iterative procedure was done in an optimization process as described later in this paper.

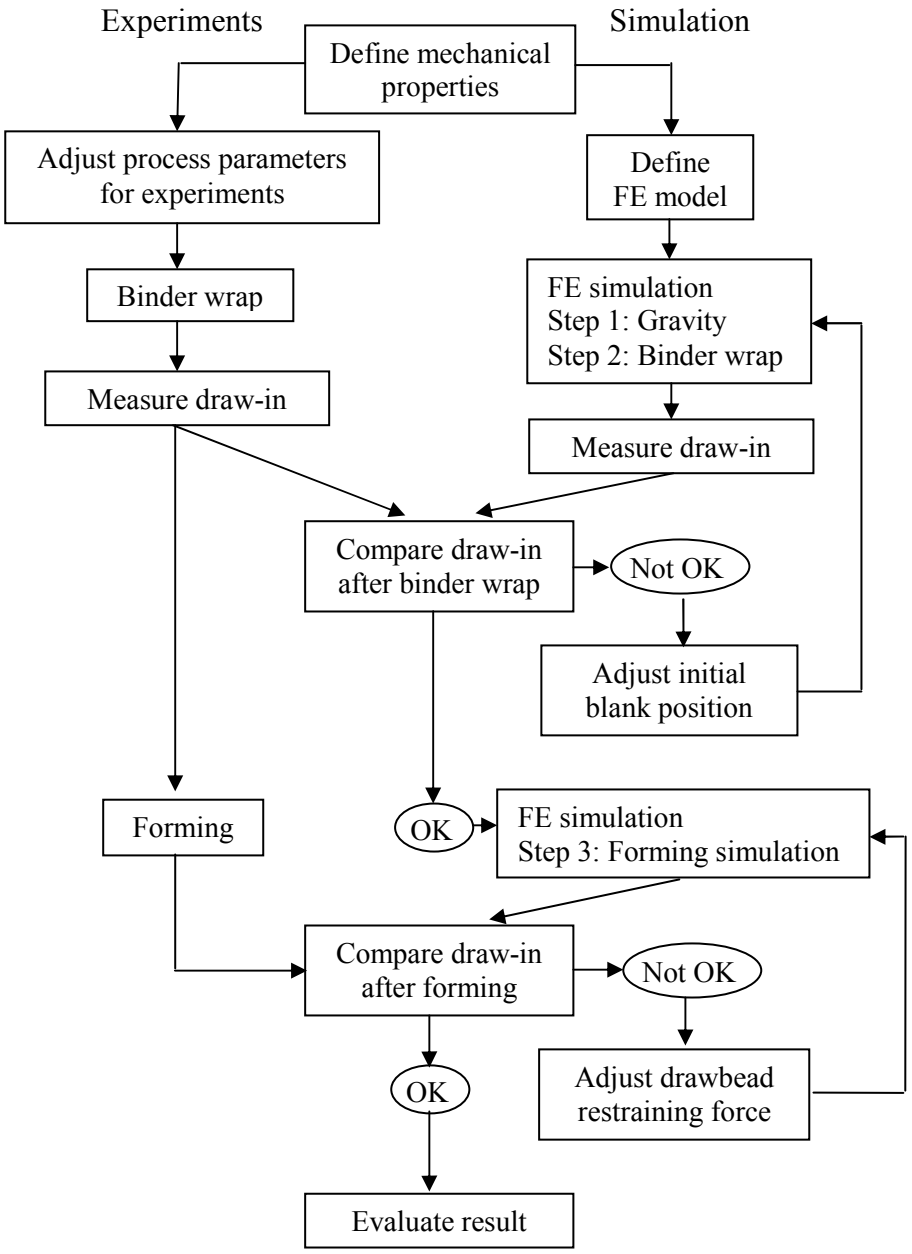

Figure 1: *Flow chart over the experimental and simulation methodology.*

2.3 Response surface methodology

The Response Surface Methodology (RSM) is a method for constructing global approximations of the objective and constraint functions based on functional evaluations at various points in the design space. The strength of the method is in

applications where gradient based methods fails, i.e. when design sensitivities are difficult or impossible to evaluate.

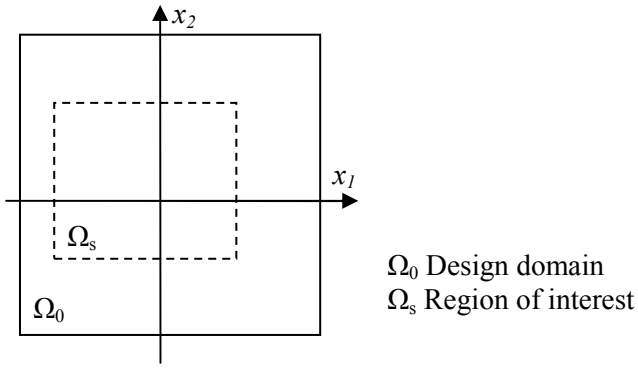

Figure 2: *Example of the design domain and the region of interest (two design variables x_1, x_2).*

The design domain is the space spanned by the design variables, i.e. $\{x_1,...,x_j\}$. The design domain can be further narrowed by introducing limits on the design variables separate from the global limits. This creates a sub-domain called the region of interest, see Figure 2, where the approximations are calculated. When the optimum is found, the region of interest is moved in the indicated direction during the next iteration and the optimization continues, see [36] for an automatic panning and zooming scheme. The selection of approximation functions to represent the actual behaviour is essential. These functions can be polynomials of any order but can also be the sum of other basis functions, e.g. sine and cosine functions.

A delicate and important task is how to distribute the experimental points in the region of interest, i.e. selecting a "Design of Experiment". The difficulty lies in the attempt of minimizing the number of simulations, but at the same time achieve a surface approximation with good quality. A popular design of experiment in structural analysis that allows the user to determine how many function evaluations that should be used is the D-optimality criterion, see [8] for further information regarding the D-optimality criterion. The D-optimality criterion has been used throughout this paper.

2.4 Space Mapping

The idea of Space Mapping is to use two models for optimization. One fine model that has a high accuracy but unfortunately is computationally expensive to solve and one coarse model that is fast to solve but has less accuracy. The Space Mapping algorithm takes advantage of the short solution time of the coarse model and the accuracy of the fine model. Therefore, the vast amount of function evaluations is performed on the coarse model and just a few corrections are made

with the fine model. The following theory for Space Mapping mainly follows [29].

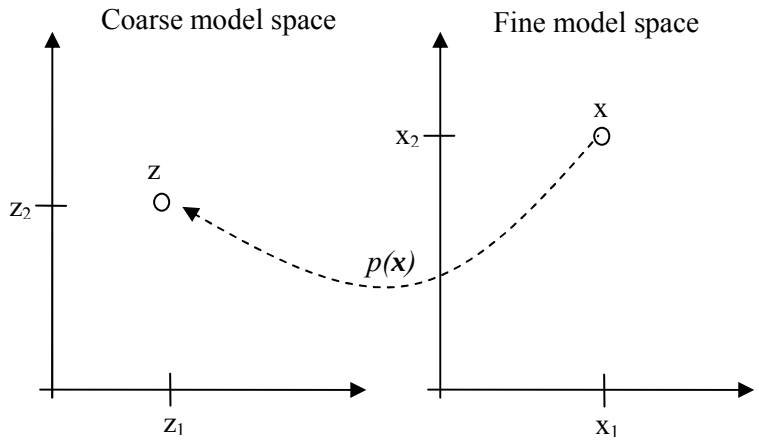

Figure 3: *Illustration of Space Mapping.*

The design parameters in the fine model is denoted $\boldsymbol{x}$ and the objective function value f_e. In the coarse model these parameters are denoted $\boldsymbol{z}$ and f_a, respectively. The optimum solution of the fine model is denoted,

$$\boldsymbol{x}^* = \arg\min_x f_e(\boldsymbol{x}). \tag{1}$$

and the optimum solution of the coarse model is denoted

$$\boldsymbol{z}^* = \arg\min_z f_a(\boldsymbol{z}). \tag{2}$$

A residual can be defined as

$$r(\boldsymbol{x},\boldsymbol{z}) = \left| f_e(\boldsymbol{x}) - f_a(\boldsymbol{z}) \right|. \tag{3}$$

A mapping function is defined that minimizes the residual,

$$p(\boldsymbol{x}) = \arg\min_z r^2(\boldsymbol{x},\boldsymbol{z}). \tag{4}$$

An illustration of the mapping function is shown in Figure 3. From the definition of the mapping function it follows that

$$f_a(p(\boldsymbol{x})) \approx f_e(\boldsymbol{x}). \tag{5}$$

The function value of the fine model is approximated with the coarse value when the mapping (3) is used as argument. Hence the coarse model can be used to minimize the fine model in (1). A perfect mapping is defined as the case when $\boldsymbol{z}^*$ satisfies $\boldsymbol{z}^*=p(\boldsymbol{x}^*)$.

The mapping p is sequentially approximated using linear approximations p_k around the current set of parameters $\boldsymbol{x}_k$. The approximation is given by

$$\boldsymbol{p}_k(\boldsymbol{x}) = \boldsymbol{z}_k + \boldsymbol{B}_k(\boldsymbol{x} - \boldsymbol{x}_k) \tag{6}$$

Here $\boldsymbol{B}_k$ is an approximation of the Jacobian of the mapping function. Following [31], we use the Broyden's update

$$\boldsymbol{B}_{k+1} = \boldsymbol{B}_k + \frac{\boldsymbol{z}_{k+1} - \boldsymbol{z}_k + \boldsymbol{B}_k\boldsymbol{h}_k}{\boldsymbol{h}_k^t\boldsymbol{h}_k}\boldsymbol{h}_k^t \tag{7}$$

where $\boldsymbol{h}_k=\boldsymbol{x}_{k+1}-\boldsymbol{x}_k$. The parameters $\boldsymbol{z}_k$ comes from (4) and hence they satisfy $\boldsymbol{z}_k=p(\boldsymbol{x}_k)$. Since the linear mapping only is valid in a neighborhood of $\boldsymbol{x}_k$, a trust region is introduced. Hence linearization is only accepted for

$$\{\boldsymbol{x} : |\boldsymbol{x} - \boldsymbol{x}_k| \langle \delta_k\} \tag{8}$$

where δ_k is the size of the trust region in step k. The trust region update procedure follows [36].

3 Experiments

The sheet metal blank used in this study consists of Rephos-steel. The basic mechanical properties are given in Table 1. R_{p02} and R_m denote the initial tensile yield stress and the ultimate tensile strength, respectively. n is the power law strain hardening exponent and R_0, R_{45} and R_{90} denote the Lankford parameters.

Table 1: *Material properties for the studied material.*

Material	**Thickness [mm]**	**R_{p02} [MPa]**	**R_m [MPa]**	**R_0, [-]**	**R_{45} [-]**	**R_{90} [-]**	**n [-]**
V-1437	1.5	278	389	1.11	0.81	1.33	0.158

3.1 Test equipment

A try-out tool for the part, denoted front side member, was used for this investigation. It is defined by CAD-data surfaces which agree well to the actual tool surfaces. The shape of a formed part can be seen in Figure 4.

The tests were performed in a 1000 metric ton hydraulic press, normally used for try-outs of production tools. The press was equipped with sensors for measuring the punch force and the blank holder force. All sensors were connected to a PC system. Figure 5 shows a picture of the tool in press.

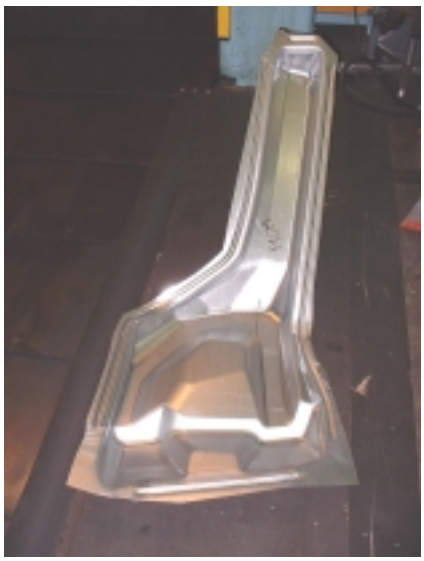

Figure 4: *Photo of the formed part.*

Figure 5: *The press tool.*

3.2 Stamping

The tool was cleaned from old lubricant and rust before the trials took place. Distance plates of 0.1 mm were used in all cases. The punch force was adjusted until a satisfactory part was obtained. Hence, the panel was stamped to the bottom without any visible cracks. All blanks were stamped without any extra lubrication. The punch forces and the draw-in for each part were noted. The average punch force was 2708 kN.

3.3 Measurements

In the measurement procedure a blank formed only by the binder wrap was used as reference. The final shape was compared to the shape after binder wrap and the draw-in was measured at the 10 locations shown in Figure 6. The draw-in was measured with an ordinary steel scale, graded every 0.5 mm. The draw-in was measured from the inner side of the drawbead perpendicular to the blank edge. The estimated measurement error is 0.25 mm.

3.3.1 Measurement after binder wrap

The perpendicular distance between the edge of the blank and the inner side of the drawbead was measured in the experimental parts on a few locations (p1, p7, p9, p15, p17 and p19 in Figure 6). These measurements verified that the initial conditions before forming were the same in the experiments and the simulations. It is of vital importance since it was the forming procedure that should be optimized.

3.3.2 Measurement of draw-in after forming

A blank taken out after binder wrap was fixated with clamps above the blank that should be measured after forming. The reference was the draw-beads, which had the same locations on both parts. After the parts were clamped together, the perpendicular distance between the parts edges was measured in the points shown in Figure 6. The results from the measurements are shown in Table 2.

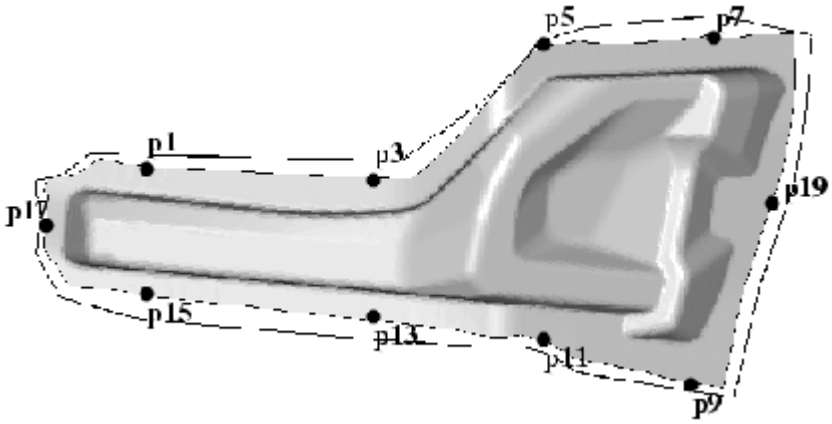

Figure 6: *Positions of the draw-in measurements.*

Table 2: *The measured draw-in and the scatter in the measurements (values in mm).*

Point	**1**	**3**	**5**	**7**	**9**	**11**	**13**	**15**	**17**	**19**
Average	22	28	18	38	23	24	32	40	18	30
Scatter	±0	±0	±0.5	±1	±1	±0	±0	±0	±2	±0.5

4 Simulation

The simulations of the forming process were performed with the FE code LS-DYNA [33]. Each simulation was divided into three steps and between each step a file with the blank properties was saved. A flow chart of the simulation procedure can be seen in Figure 7. The gravity simulation was done using implicit time integration and the binder wrap and forming simulations were done using explicit time integration. Between the gravity and the binder wrap the blank mesh was uniformly refined and after the binder wrap another uniform refinement was done. The final element size was about half the draw radius.

The advantage with the above strategy is that it reduces the calculation time, since only the forming part of the process can be used in the optimization. This means that e.g. the time consuming binder wrap operation just need to be simulated once.

The blank was modelled by Belytschko-Lin-Tsay quadrilateral shell elements [34]. The 3-parameter Barlat material model in LS-DYNA, developed by Barlat and Lian [35], was used, and the m-value was chosen to 8. The drawbeads were modelled by a constant restraining force.

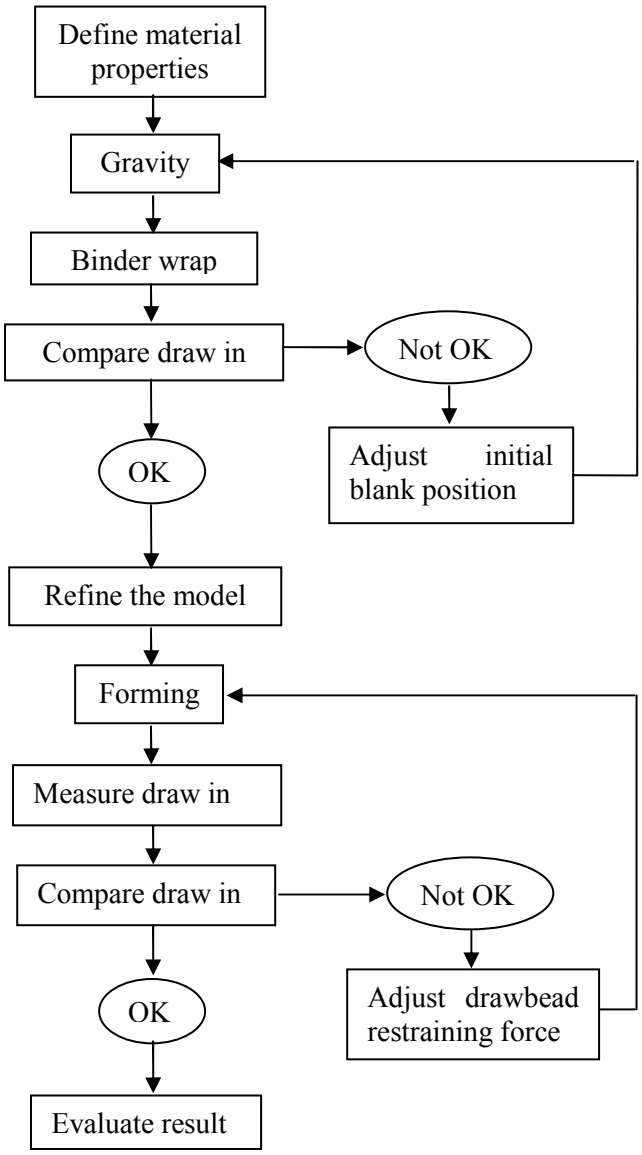

Figure 7: *Flow chart of the simulation procedure.*

The FE model used in the simulations is shown in Figure 8.The model consists of 50391 shell elements. The CPU time for the forming part of the process was approximately 35 minutes on an IBM power 3, 375 MHz computer using 16 processors and 3.5 hours on a Linux 800 MHz PC.

4.1 Drawbead description

The modelled drawbeads were divided into straight sections. These sections had a unique restraining force, which were tuned towards the measured draw-in in the corresponding sections. The locations of the equivalent drawbeads are shown in Figure 9.

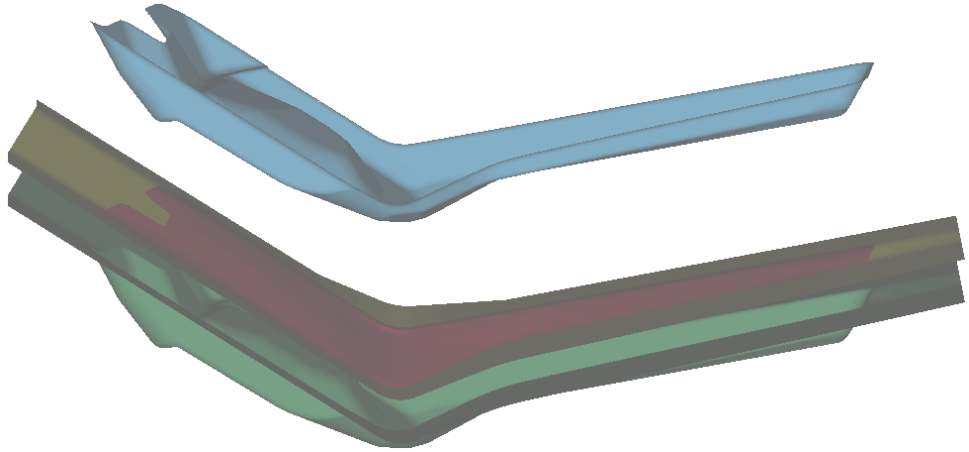

Figure 8: *The FE model used in the optimization procedure.*

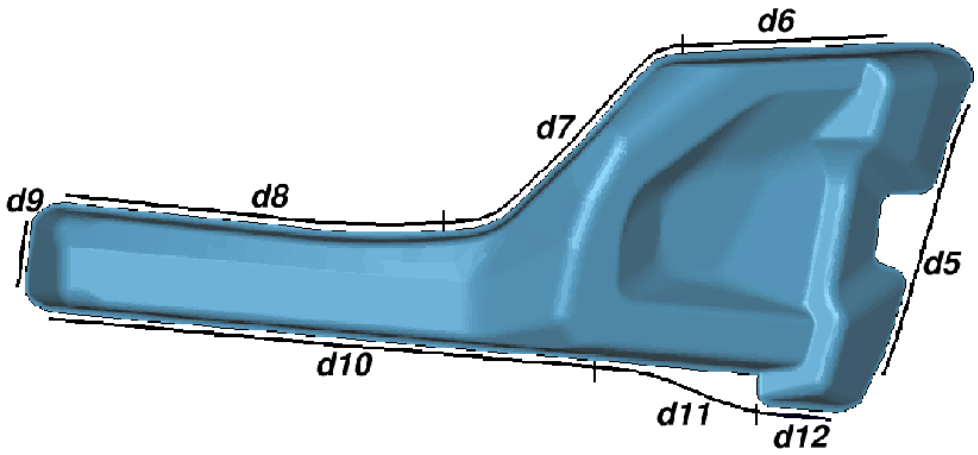

Figure 9: *Equivalent drawbead locations in the FE model.*

5 The draw-in optimization

To be able to compare the classical Response Surface Methodology with the Space Mapping technique the optimization was conducted using each of the methods.

Two Space Mapping optimizations were performed. In the first Space Mapping optimization (SM1) response surfaces from the first RSM iteration were used as the coarse model for the subsequent iterations. In the second (SM2) optimization response surfaces from the second RSM iteration were used.

The expected result was that RSM should find a good solution, but at the cost of many iterations. The Space Mapping method should be much faster than RSM, but the optimal solution might not be as accurate. Due to the inaccurate surfaces used in SM1, SM2 should give a better result compared to SM1.

As illustrated in Figure 7 only the forming part of the process was simulated for each set of variables.

5.1 Problem description

The problem in the draw-in optimization was to find the set of drawbead parameters (d_5, ..., d_{12}) that minimizes the sum of the differences between the measured and simulated draw-in. Bounds on the draw-in were also added with a tolerance of ±1 mm. The optimization problem was stated as,

$$\min_{d_5,\ldots,d_{12}} \sum_{i=1}^{10} \left(abs(in_i) - abs(target_i)\right)$$

$$s.t.\ lb_i \le in_i \le ub_i$$

$$0 \le d_i\ 800N/mm \quad i = 1,\ldots,8$$

where in_i is the draw-in from the FE simulation and $target_i$ is the draw-in measured in the experiment. $target_i$, lb_i (lower bound) and ub_i (upper bound) are defined in Table 3.

Table 3: *Upper and lower bounds on the draw-in responses (values in mm).*

Point	**1**	**3**	**5**	**7**	**9**	**11**	**13**	**15**	**17**	**19**
target$_i$	22	28	18	38	23	24	32	40	18	30
lb$_i$	21	27	17	37	22	23	31	39	17	29
ub$_i$	23	29	19	39	24	25	33	41	19	31

6 Result

The results from the optimizations are shown in figures 10 and 11. Two optimizations were conducted with the Space Mapping technique. One with response surfaces from the first RSM iteration (SM1) and one with surfaces from the second RSM iteration (SM2).

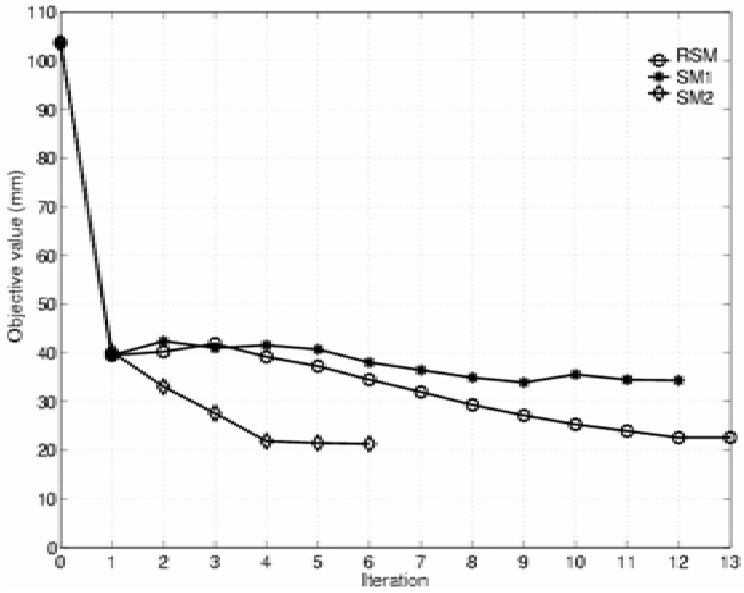

Figure 10: *Objective history.*

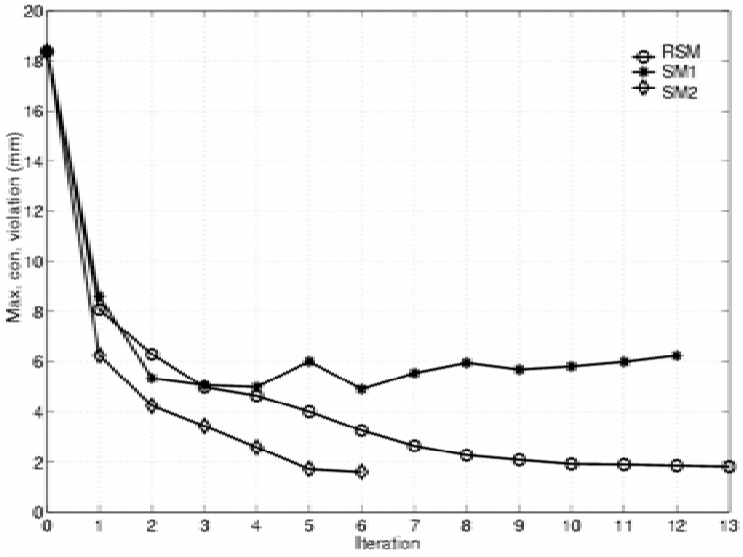

Figure 11: *Maximum constraint violation history.*

As expected the draw-in at the optimum point achieved by SM1 differs most from the physical test and this solution ends up at an incorrect optimal point, which violates the constraints too much. As seen in Figure 10 SM2 actually converges to a better objective value, hence the draw-in is better calibrated, compared to the RSM optimization. The maximum constraint violation in Figure 11 follows the same trend as the objective value.

In Table 4 the initial and optimum draw-in for the three optimizations are stated. The optimum draw-in for RSM and SM2 are almost identical but SM2 converges to a slightly lower total difference in draw-in. When Space Mapping is used in SM2 the required computing time is drastically reduced by a factor of 5.3.

Table 4: *Initial and optimum draw-in (values in mm).*

	in_1	in_3	in_5	in_7	in_9	in_{11}	in_{13}	in_{15}	in_{17}	in_{19}	obj	con	sim
Target	22	28	18	38	23	24	32	40	18	30			
Start	47.6	47.4	21.7	45.6	22.2	16.1	19.5	21.9	11.7	31.9	107	24.6	1
RSM	22.7	30.8	15.2	40.8	25.8	21.2	34.5	42.8	17.3	32.0	22.6	1.82	183
SM1	23.8	30.5	14.0	39.8	26.9	21.9	36.1	43.6	25.2	33.3	34.3	6.23	26
SM2	20.5	30.3	15.6	40.1	25.4	22.0	34.0	42.6	15.8	31.7	21.3	1.61	34

The achieved drawbead restraining forces are stated in Table 6. Even though the draw-in of RSM and SM2 in Table 4 are almost identical the optimization methods do not converge to the same optimal set of design variables. This illustrates that the optimization problem has several local optima and depending on the chosen method and starting point the methods converge to different optimal points. Hence, it is never possible to guarantee that the reached optimal point is the true global optimal solution.

6.1 Comparison with physical beads

A comparison between the restraining forces achieved from the optimal solution and the restraining forces in the physical tool was made. First the geometry of the drawbeads was measured in the tool. Then a FE model of the drawbead was used to determine the restraining force.

The FE model used for studying the drawbead forces was similar to what was used in [37] and [38]. The drawbead was fully parametrized by using the pre-processor TrueGrid, see [39]. The geometry design parameters *w, t, c, rc, rb* and *h*, see Figure 12, were used. The simulation lay-up is shown in Figure 12. The simulation model consists of a 5 mm wide sheet that is drawn with a prescribed velocity through a drawbead. Constraints on the sheet were added such that a plane strain condition was achieved in the transverse direction. The restraining force is measured with a section force in the blank.

The size of the drawbeads are shown in Table 5 together with the resulting restraining forces. In Table 6 the resulting restraining forces from the optimizations are shown.

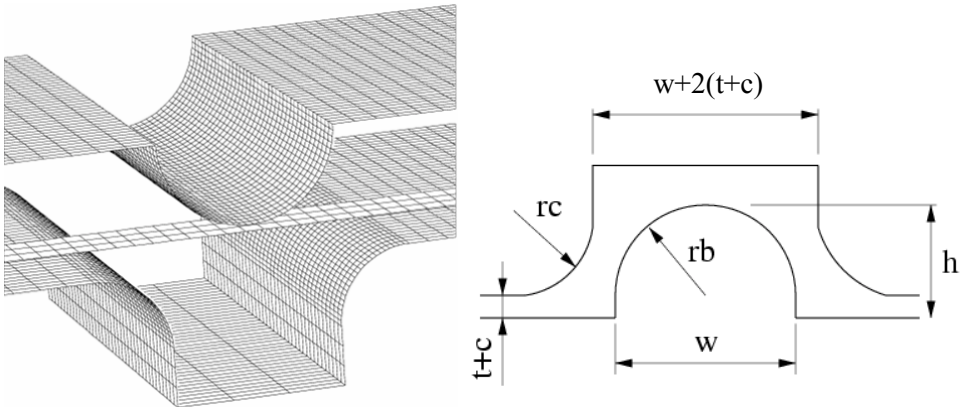

Figure 12: *Simulation lay-up and parameters in the drawbead.*

Table 5: *Measured drawbead geometries in the physical tool (values in mm).*

Drawbead	**d_5**	**d_6**	**d_7**	**d_8**	**d_9**	**d_{10}**	**d_{11}**	**d_{12}**
Rb	6	7	12	6	6	6	7	7
Rc	5	5	5	5	5	5	5	5
H	6	5	3	6	6	6	4	4.5

Table 6: *Resulting optimal force from the optimization and measured force (values in N/mm).*

	$F(d_5)$	**$F(d_6)$**	**$F(d_7)$**	**$F(d_8)$**	**$F(d_9)$**	**$F(d_{10})$**	**$F(d_{11})$**	**$F(d_{12})$**
Start	350	350	300	400	400	400	400	200
RSM	346	439	277	445	404	393	345	198
SM1	323	452	296	411	288	372	349	167
SM2	345	450	248	478	439	407	298	282
Measured	412	394	342	412	412	412	392	392

7 Conclusions

An optimization of the draw-in of an automotive sheet metal part has been carried out using the Response Surface Methodology (RSM) and the Space Mapping technique. The optimization adjusts the drawbead restraining force in the FE model such that the draw-in from the simulation is the same as the draw-in in the physical process. Both optimization methods used in this work are successful in optimizing the draw-in. The best solution is reached when the Space Mapping method is used with reasonably accurate response surfaces. This method also drastically reduces the required computing time compared to RSM.
As seen in tables 5 and 6 a perfect match between the optimized restraining force and the actual restraining force in the tool has not been reached. However, the restraining force from RSM differs approximately at most 15% except in point 12. The cause of the difference is either that the drawbeads are not measured correctly, the draw-in is not measured in the same way in the tests as in the simulations, the material model does not correspond to the actual material or the friction properties differ between the tooling and the FE model. In the FE model a Coulomb friction model has been used with a friction coefficient of 0.15 on the entire tool. Perhaps this coefficient is too high and the friction properties may be different in different sections of the tool. Nevertheless, judging by the result the optimization methods give results that are close to what has been observed in the physical test.

The conclusions of this study is that Space Mapping is a very effective and accurate method to use when calibrating the draw-in of a sheet metal forming process.

Acknowledgements

This work is performed within the Simuform project. The project is funded by the Swedish Foundation for Strategic Research, programme ProViking. The work was also financially supported by Volvo Cars Body Components and the Swedish Foundation for Strategic Research, programme PROPER. Volvo Cars Body Components has provided the sheet metal forming model. We acknowledge Dr. Nielen Stander (LSTC) for fruitful discussions on optimization methods and the optimization package LS-OPT. At last we wish to thank Professor Jan-Eric Ståhl (Division of Production and Materials Engineering, Lund University) for his encouragement and support.

References

[1] Makinouchi, A., Sheet metal forming simulation in industry, *Journal of Materials Processing Technology* **60** (1996) 19-26.

[2] Makinouchi, A., Teodosiu, C. and Nakagawa, T., Advance in FEM simulation and its related technologies in sheet metal forming. *CIRP Annals - Manufacturing Technology* **47(2)** (1998) pp. 641-649.

[3] Andersson, A., Use of FE-analysis in predicting and verifying the design of an automotive component forming process, with special regard to macro geometric defects. Licentiate thesis, Div of Prod. and Mat. Eng., LTH, Lund, 2001.

[4] Fratini, L. and Micari, F., Investigating effective blank holder force paths to improve the maximum component height in deep drawing processes. *Numisheet '99*, Besancon, 1999.

[5] Lin, Z-Q., Bao, Y-X., Chen,G-L. and Liu, G., Study on the drawbead setting of the large deformation and bending area in a cover panel. *Numisheet '99*, Besancon, 1999.

[6] Meinders, T., Carleer, B., Geijselaers, H., and Huétink, J., The implementation of an equivalent drawbead model in a finite-element code for sheet metal forming. *Journal of Materials Processing Technology* **83** (1998), pp. 234-244.

[7] Naceur, H., Guo, Y., Batoz, C., and Knopf-Lenoir, C., Optimization of drawbead restraining forces and drawbead design in sheet metal forming process. *Int. J. Mech. Sci.* **43** (2001), pp. 2407-2434.

[8] Myers, R. and Montgomery, D., *Response Surface Methodology*. John Wiley, New York, 1995.

[9] Roux, W., Stander, N., and R.T., H., Response surface approximations for structural optimization. *International Journal for Numerical Methods in Engineering* **42** (1998), pp. 517-534.

[10] Stander, N., Roux, W., Pattabiraman, S. and Dhulipudi, R., Response surface approximations for design optimization problems in nonlinear dynamics. *ASME Pressure Vessels and Piping Conference Boston* 1999, PVP-99-0304524-7;396, pp. 275-284, 1999.

[11] Kok, S. and Stander, N., Optimization of a sheet metal forming process using successive multipoint approximations. *Structural Optimization* **18** (1999), pp. 277-295.

[12] Abe, Y., Mori, K. and Ebilhara, O., Optimisation of the distribution of wall thickness in the multistage sheet metal forming of wheel disks. *J. Mater. Process. Technol.* **125-126** (2002), pp. 792-797.

[13] Doege, E. and Elend, L.-E., Design and application of pliable blank holder systems for the optimization of process conditions in sheet metal forming. *J. Mater. Process. Technol.* **111** (2001), pp. 182-187.

[14] Gantar, G., Pepelnjak, T. and Kuzman, K., Optimization of sheet metal forming processes by the use of numerical simulations. *J. Mater. Process. Technol.***130-131** (2002), pp. 54-59.

[15] Guo, Y.Q., Batoz, J.L., Naceur, H., Bouabdallah, S., Mercier, F. and Bartlet, O., Recent developments on the analysis and optimum design of sheet metal forming parts using a simplified inverse approach. *Computers and Structures* **78** (2000), pp 133-148.

[16] Hino, R., Yoshida, F. and Toropov, V., Optimization of blank design for deep drawing process based on the interaction of high and low fidelity models. 9th AIAA/ISSMO *Symposium on Multidisciplinary Analysis and Optimization 4-6 September 2002*, Atlanta, AIAA 2002-5564, 2002.

[17] Jensen, M.R., Damborg, F.F., Nielsen, K.B. and Danckert, J., Optimization of the draw-die design in conventional deep-drawing in order to minimise tool wear. *J. Mater. Process. Technol.* **83** (1998), pp. 106-114.

[18] Kim, J.-Y., Kim, N. and Huh, M.-S., Optimum blank design of an automobile sub-frame. *J. Mater. Process. Technol.* **101** (2000), pp. 31-43.

[19] Kubli, W. and Reissner, J., Optimization of sheet-metal forming processes using the special-purpose program AUTOFORM. *J. Mater. Process. Technol.* **50** (1995), pp. 292-305.

[20] Ohata, T., Nakamura, Y., Katayama, T., Nakamachi, E. and Nakano, K., Development of optimum process design systems by numerical simulation. *J. Mater. Process. Technol.*, **60** (1996), pp. 543-548.

[21] Park, S.H., Yoon, J.W, Yang, D.Y and Kim, Y.H., Optimum blank design in sheet metal forming by the deformation path iteration method. *Int. J. Mech. Sci.* **41** (1999), pp. 1217-1232.

[22] Pepelnjak, T., Gantar, G. and Kuzman, K., Numerical simulations in optimization of product and forming process. *J. Mater. Process. Technol.* **115** (2001), pp. 122-126.

[23] Santos, A.D., Duarte, J.F., Reis, A., da Rocha, B., Neto, R. and Paiva, R., The use of finite element simulation for optimization of metal forming and tool design. *J. Mater. Process. Technol.* **119** (2001), pp. 152-157.

[24] Shim, H., Son, K. and Kim, K., Optimum blank shape design by sensitivity analysis. *J. Mater. Process. Technol.* **104** (2000), pp. 191-199.

[25] Sosnowski, W., Marczewska, I. and Marczewski, A., Sensitivity based optimization of sheet metal forming tools. *J. Mater. Process. Technol.* **124** (2002), pp. 319-328.

[26] Stander, N., The Successive Response Surface Method Applied to Sheet-Metal Forming. In: Bathe, K.J. (ed) *The First MIT Conference on Computational Fluid and Solid Mechanics (Boston, June 12-15, 2001)*, Oxford, Elsevier Science Ltd, 2001.

[27] Stander, N., Springback Compensation in Sheet Metal Forming Using a Successive Response Surface Method. *9th AIAA/ISSMO Symposium on Multidisciplinary Analysis and Optimization 4-6 September 2002*, Atlanta, AIAA 2002-5539, 2002.

[28] Bakr, M., Bandler, J., Madsen, K., Rayas-Sánchez, J., and Sondergaard, J., Space mapping optimization of microwave circuits exploiting surrogate models. *IEEE Trans. Microwave Theory. Tech.* **48** (2000), pp. 2297-2306.

[29] Leary, S., Bhasker, A., and Keane, A., A constraint mapping approach to the structural optimization of an expensive model using surrogates. *Conference on Surrogate Modelling and Space Mapping for Engineering Optimization*, Lyngby, 2000.

[30] Redhe, M. and Nilsson, L., Using space mapping and surrogate models to optimize vehicle crashworthiness design, AIAA-2002-5536, Editor Farrokh Mistree. *9th AIAA/ISSMO Symposium on Multidisciplinary Analysis and Optimization*, Atlanta, 2002.

[31] Madsen, K. and Sondergaard, J., Space mapping from a mathematical viewpoint. *Conference on surrogate modelling and space mapping for engineering optimization*, Lyngby, 2000.

[32] Jansson, T., Nilsson, L and Redhe, M., Using surrogate models and response surfaces in structural optimization -with application to crashworthiness design and sheet metal forming. *Struct. Multidisc. Optim.*, **25(2)**, (2003), pp. 129-140.

[33] Hallquist, J.O., LS-DYNA *Theoretical Manual.* Livermore Software Technology Coporation, Livermore, 1998.

[34] Belytschko, T., Lin, J. and Tsay, C.S., Explicit algorithms for nonlinear dynamics of shells. *Comp. Meth. Appl. Eng.* **42** (1984), pp. 225-251.

[35] Barlat, F. and Lian, J., Plastic behaviour and strechability of sheet metals. Part I: A yield function for orthotropic sheet under plane stress conditions. *Int. J. of Plasticity* **5** (1989),pp. 51-66.

[36] Stander, N, Craig K.J and Roux, W., LS-OPT User's Manual v. 2. Livermore Software Technology Corporation, Livermore, 2002.

[37] Nilsson, D. and Trana, K., *FE-analys av dragvulster -Implementering av dragvulster inom plåtformingssimulering*. CODEN:LUTMDN/(TMMV-5129)/1-90/1998. Inst. för Mekanisk Teknologi och Verktygsmaskiner, Lunds Tekniska Högskola, 1998 (in swedish).

[38] Mattiasson, K. and Larsson, M., *Numerical procedures for 2D drawbead simulation*, Department of Structural Mechanics, Chalmers University of Technology. Göteborg, 2001.

[39] XYZ Scientific Applications inc. *TrueGrid Manual.* XYZ Scientific Applications inc., Livermore, 2001.